10.3233/BME-201171

Investigation of Two-Way Fluid-Structure Interaction of Blood Flow in a Patient-Specific Left Coronary Artery

Abdulgaphur Athani[1], N.N.N Ghazali[1], Irfan Anjum Badruddin[2,3], Sarfaraz Kamangar[3], Ali E Anqi[3], Ali Algahtani [2,3]

[1]*Department of Mechanical Engineering, Faculty of Engineering, University of Malaya, 50603 Kuala Lumpur, Malaysia*
[2]*Research Center for Advanced Materials Science (RCAMS), King Khalid University, Abha-61413, Asir, Kingdom Saudi Arabia*
[3]*Mechanical Engineering Department, College of Engineering, King Khalid University, Abha-61411, Asir, Kingdom Saudi Arabia*

Corresponding author: nik_nazri@um.edu.my, magami.irfan@gmail.com

ABSTRACT

The blood flow in the human artery has been a subject of sincere interest due to its prime importance linked with human health. The hemodynamic study has revealed an essential aspect of blood flow that is eventually proving to be of paramount importance to make a correct decision to treat patients suffering from cardiac disease. The current study aims to elucidate the two-way fluid-structure interaction (FSI) analysis of the blood flow and the effect of stenosis on hemodynamic parameters. A patient-specific 3D model of the left coronary artery was constructed based on computed tomography (CT) images. The blood is assumed to be incompressible, homogenous, and behaves as Non-Newtonian, while the artery is considered as a nonlinear elastic, anisotropic, and incompressible material. Pulsatile flow conditions were applied at the boundary. Two way coupled FSI modeling approach was used between fluid and solid domain. The hemodynamic parameters such as the pressure, velocity streamline, and wall shear stress were analyzed in the fluid domain and the solid domain deformation. The simulated results reveal that pressure drop exists in the vicinity of stenosis and a recirculation region after the stenosis was found. It was also noted that stenosis leads to high wall stress. The results also demonstrate an overestimation of wall shear stress and velocity in the rigid wall CFD model compared to the FSI model.

Keywords: Left coronary artery, Image processing, CFD, FSI, Blood flow modelling**.**

1. Introduction

In the year 2016, World Health Organization reported an estimation of 17.9 million deaths by cardiovascular diseases, which accounts for almost 31% of the total annual deaths. Atherosclerosis is a chronic coronary artery disease that results in the restriction of blood flow to the heart's muscles. Many studies showed that the hemodynamic forces play a vital

role in the variation of morphology and physiology of coronary arteries. Several researchers suggested that the morphology of the artery changes due to the formation of plaque (stenosis), which occurs across the curved and bifurcated sections where the wall shear stresses are very low [1]. The wall of an artery is mainly composed of three different types of layers. The innermost layer is called tunica intima (which is lined by smooth tissue endothelium), tunica media (the muscular middle layer), and the tunica adventitia (outermost layer). The continuous exposure of the luminal surface (tunica intima) and endothelium layer to blood flow produces the hemodynamic shear forces [2-4]. When these hemodynamic forces are inadequate to maintain the physiological range, it leads to stenosis initiation and progression. Many engineers, clinicians, and mathematical researchers have carried out substantial work on the effect of stenosis severity on the blood flow [5-9]. Despite recent advancements in non-invasive medical image processing such as Magnetic Resonance Imaging (MRI) and coronary computed tomography angiography (CCTA), finding the blood flow pattern remains challenging. The anatomical reconstruction of the coronary artery wall can be determined using these imaging techniques but is limited to find the hemodynamic factors non-invasively.

In contrast, computational fluid dynamics analysis enables the recognition of hemodynamic changes and the progression and development of stenosis in the coronary artery. Due to the highly complex structure of the artery wall and limitation in the experimental and computation methods developed, the progression and plaque development are still not clearly understood. Numerous studies related to the blood flow patterns and wall shear stress (WSS) have been reported to improve the understanding of the growth of stenosis by using patient-specific medical images[10,11]. These studies show that the accurate reconstruction of the blood domain can be achieved, and the momentum and continuity equations could be solved numerically. The magnitudes of stress and strain inside the artery wall can also be computed by modeling the fluid-structure interaction. The effect of the fluid domain on the wall of structural domain vise-versa can be modeled by two-way fluid-structure interaction [12]. The main goal of the current study is to understand the mechanism of progression and growth of a plaque inside the artery wall and to identify the site of rupture by using the patient-specific left coronary artery.

2. Methodology

2.1 Medical Image-Based Geometrical Reconstruction of Left Coronary Artery model

The left coronary artery of an alleged patient of the male was selected to obtain the computed tomography (CT) images data. The CT scanned images were obtained by using 128-multislice. The standard protocol was adopted to obtain the CT images of the patient. Interval of reconstruction was 0.6mm and Beam collimation 0.6 with pitch 1.4 along with tube voltage of 100 kV, current oscillating from 300 to 650mAs.

The images were reconstructed in the axial directions having a slice thickness of 0.6mm with a total distance of 0.75mm. The images in all the directions (coronal, sagittal, and axial planes) had more than 400 slices. The collected images are taken in a standard DICOM format, and then a realistic 3D left coronary artery model was rebuilt with the help of CT volume data using image processing software MIMICS-18 [9]. Figure 1 shows the CT scan images and the 3D volume rendering image of the left coronary artery model.

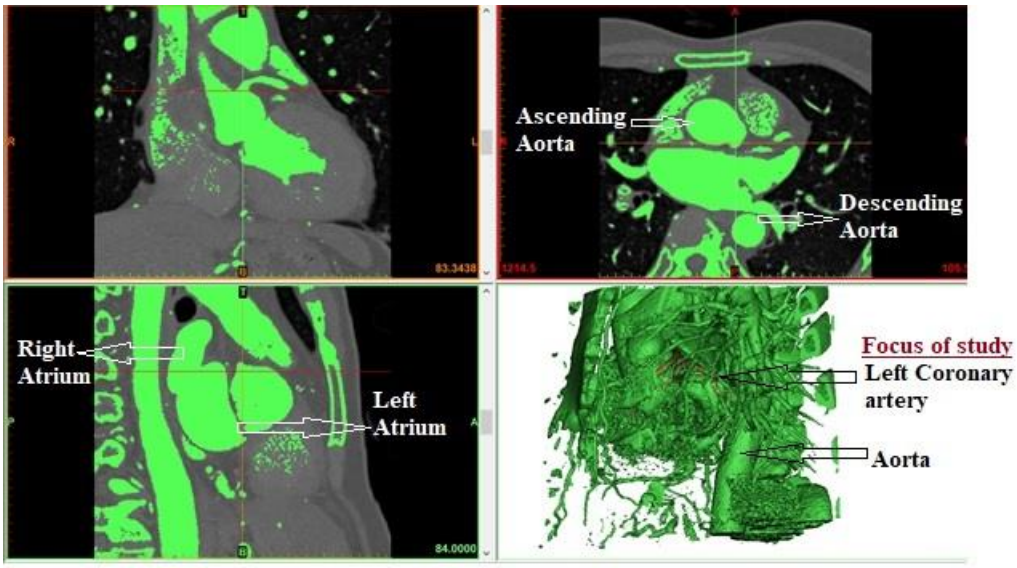

Fig. 1: Procedure of patient's specific reconstruction of left coronary artery from the CT scan images

2.2 3D modeling

The CT scan images obtained from the patient with stenosis in the left coronary artery were exported to stl. format via MIMICS 18 software. The reconstruction of the left coronary artery was achieved by defining a series of appropriate thresholds ranging from 84 to 630 HU. The left coronary artery was identified, and the segmentation process was carried out. The detailed segmentation process of left coronary artery models, as shown in Figure 1, is explained in the literature [11]. The reconstructed 3-dimensional models were imported into ANSYS. As the FSI model consists of fluid and solid domains representing blood and wall, both were generated separately. As shown in figure (2), the geometry of the blood domain

was used for the CFD analysis as it only represents the blood domain. As shown in figure (3), the structural domain was subsequently built with ANSYS space claim software by balancing the fluid domain surfaces shown in figure 2. The wall thickness of 0.4mm was considered for the Left coronary artery. The 3D blood domain and wall models meshed separately (figure 4). The dimensions of the left coronary artery model are as shown in the table 1.

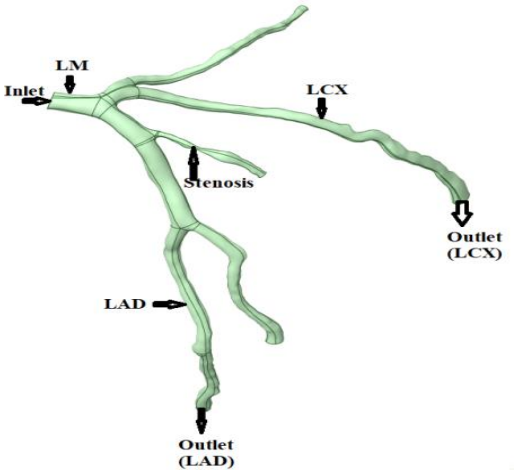

Fig. 2: 3D blood domain of left coronary artery

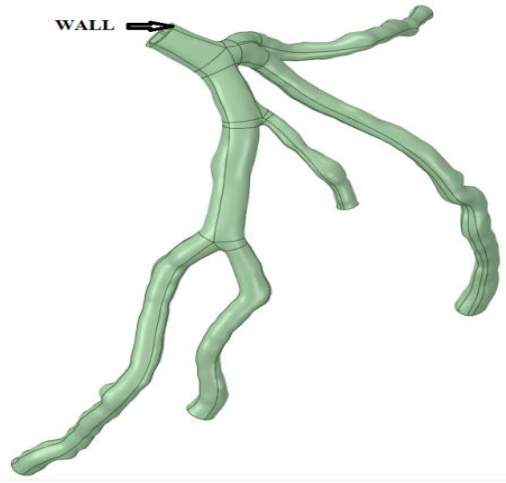

Fig. 3: 3D structural domain of left coronary artery

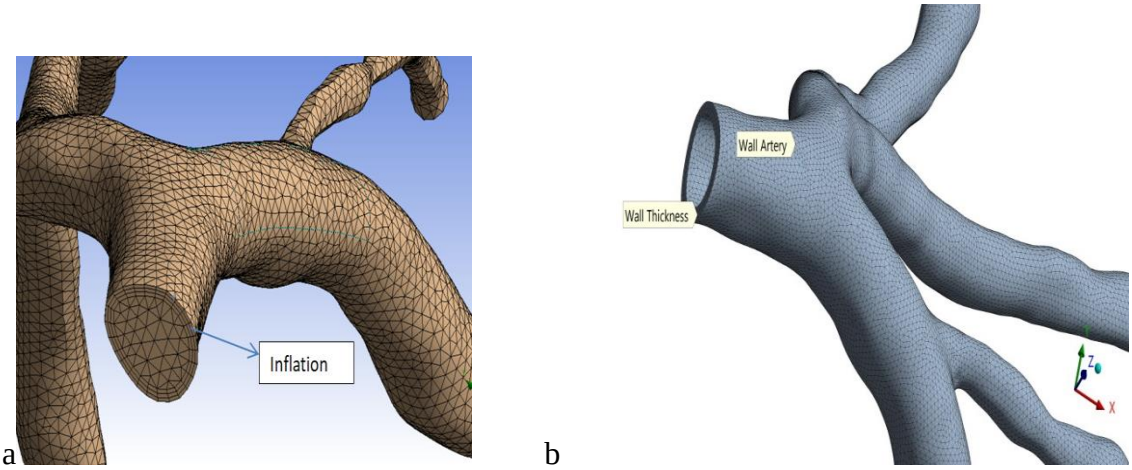

a b

Fig.4: Tetrahedral and uniform mesh for the a) blood domain and b) Structural domain

Table1: Dimensions of the reconstructed left coronary artery

Length of LM	9.91mm
Length of LCx	66.27mm
Length of LAD	82.29mm
Vessel wall thickness	0.4mm
Diameter of LM (Inlet)	3.186mm
Diameter of LAD (Outlet)	2.168mm
Diameter of LCx (Outlet)	2.823mm
Area of inlet (LM)	7.9715mm2
Angulation between LCx and LAD	78.48^{o}

2.3 Mesh independent study

An automatic meshing algorithm was selected in the first stage to obtain the discretized fluid domain in ANSYS Meshing. The Tetrahedron mesh method was used in order to get a smooth and uniform mesh. The fluid domain meshed is 869,825 tetrahedral elements, and the structural domain with the same elements of 726,563. Thus a total of 1596,388 tetrahedral mesh elements were used in the Fluid-Structure Interaction, as depicted in figure 4a and figure 4b. Furthermore, the mesh was refined by adding the inflation layers across the interface between the fluid and structural domains to get more precise results in areas near the artery walls, as shown in figure 4a. An independent grid study was also performed, with figure 5 representing the detailed grid study.

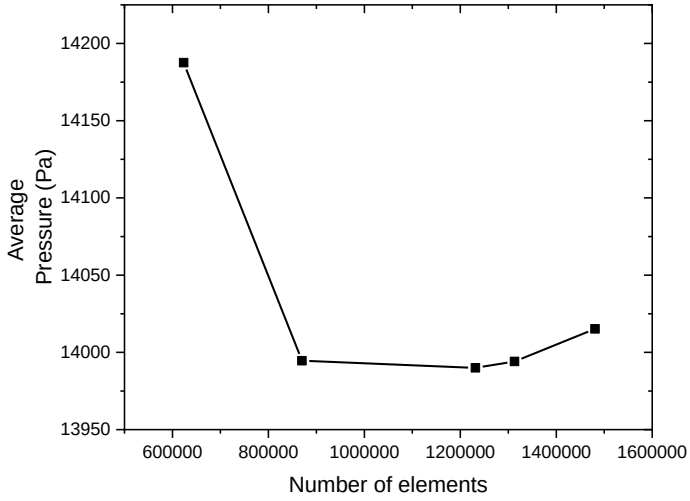

Fig. 5: Mesh independent study

The results of figure 5 show a decrease in average pressure from the number of mesh elements 623,279 to 1480,875 in the fluid domain. Moreover, 20% higher elements took about 200% additional time, but the variances in the wall pressure are found to be insignificant. The transient CFD analysis was performed with FLUENT, with a maximum number of 20 iterations. The convergence criteria were accepted when the residuals were below $10e^{-5}$. Each simulation was achieved over two cardiac.

2.4 Boundary conditions

The boundary condition is the essential step of the engineering design system. It is impossible to discretize the entire cardiovascular system if the region or areas analyzed do not have one inlet and one outlet condition. The blood supply to the heart takes place during diastole but not at systolic conditions, and most researchers said that the use of cardiac cycles at inflow and outflow conditions is more important [13-15]. Time-dependent velocity profiles were applied at the inlet according to the literature [16-19] as shown in figure (6), and an average pressure of 13,300 [Pa] was applied at the outlets [20]. The inflow and outflow have been imposed with zero displacements for the adjacent faces, relatively to the structural domain. Other boundaries of the structural domain are applied with a condition of free deformation, which permits the structural domain to deform in all the directions.

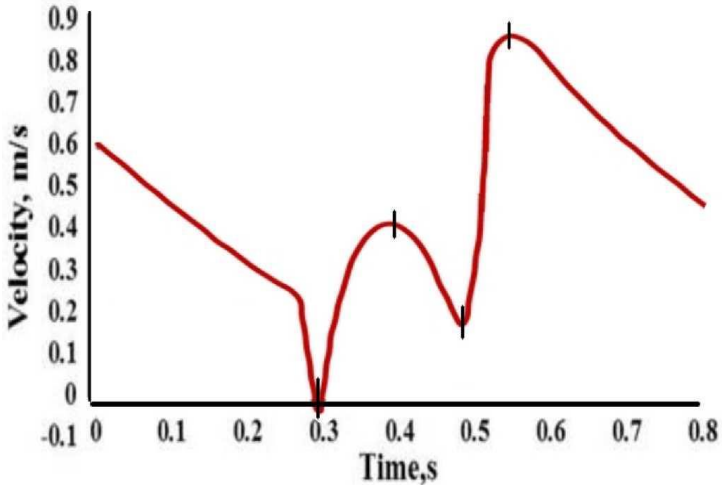

Fig. 6: Inlet pulsatile velocity profile of coronary cardiac cycle [17,19,18,16]

2.5 Blood flow modeling

Blood flow in the left coronary artery was considered as homogenous, incompressible, and Non-Newtonian [21,8,22]. Hence, the governing equations are given as:

$$\rho_f \nabla . \vec{V} = 0 \quad \ldots\ldots\ldots\ldots\ldots\ldots\ldots\ldots\ldots\ldots 1$$

$$\frac{\partial \vec{V}}{\partial t} + \rho_f \left(\vec{V}.\nabla\right)\vec{V} = -\nabla p + \nabla \bar{\bar{\tau}} \quad \ldots\ldots\ldots\ldots .. 2$$

where, ρ_f is the Density of fluid $\vec{V}$ is the Velocity Vector, "t" represents time and "p" represent the fluid pressure and $\bar{\bar{\tau}}$ is the viscous shear tensor.

The above Eq. (1) represents that the rise in local density with time is balanced with a divergence of mass flux and Eq. (2) represents the momentum change with time in a fluid particle is equal to the summation of the forces present on it. The fluid-particle forces are taken as viscous and pressure forces, denoted in the RHS (Right Hand Side) of Eq. (2), whereas body forces like gravity have been neglected. As per the previous studies [23,24], the fluid behavior is considered to be Non-Newtonian in vessels; this approximation is followed because of the vessel's diameters. Typically, these diameters are more prominent when compared with the diameters of individual red blood cells [25,26], making the blood viscosity independent of the shear rate. The shear rate is more significant in coronary arteries, around 100m/s, and kept a flow system with constant viscosities [27,28].

2.6 Artery deformation modeling

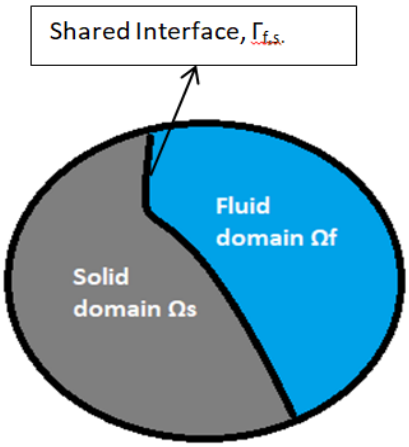

Fig. 7: Fluid-structure Interaction domains and Boundary Interface

Figure 7 depicts a systematic Fluid Structural interaction problem with a solid Ω_s and fluid domain Ω_f, which are self-governing from each other and interrelate alongside with common shared interface, $\Gamma_{f,s}$

The equation which governs the wall deformation of a vessel is, Eq. (3)

$$\rho_s \frac{\partial^2 u}{\partial t^2} - \nabla \bar{\bar{\sigma}} = \rho_s \vec{b} \quad \ldots\ldots\ldots\ldots\ldots\ldots\ldots\ldots 3$$

Where, "ρ_s" the structure density, "u" represents the solid Displacements, "$\bar{\bar{\sigma}}$" represent the Cauchy stress tensor, and $\vec{b}$ is body force. The stress tensor is given as:

$$\bar{\bar{\sigma}} = 2\mu_L \bar{\bar{\epsilon}} + \lambda_L tr(\bar{\epsilon}) I \quad \ldots\ldots\ldots\ldots\ldots\ldots 4$$

Where, λ_L *and* μ_L are the first and second-order Lame parameters respectively, " $\bar{\bar{\epsilon}}$ " is the strain tensor, word "tr" represents the trace function, and "I" represents the characteristics matrix.

$$\mu_L = \frac{E}{2(1+\vartheta)} \quad \ldots\ldots\ldots\ldots\ldots\ldots\ldots\ldots\ldots\ldots\ldots\ldots 5$$

$$\lambda_L = \frac{\vartheta E}{(1+\vartheta)(2\vartheta-1)} \quad \ldots\ldots\ldots\ldots\ldots\ldots\ldots\ldots 6$$

2.7 Fluid-Structure interaction modeling (FSI)

FSI coupling is performed by the construction of two separate models that comprised the fluid and structural domains. In solving the FSI problems, neither Eulerian nor the

Lagrangian formulations are primes to both the domain. The Lagrangian formulation cannot handle large deformations for the fluid, whereas Eulerian formulation compromises accuracy when applied to the solid domain. Generally, the FSI was resolved using a standard Arbitrary Lagrangian-Eulerian (ALE) formulation [29]. The fluid domain is permitted to deform arbitrarily in the ALE method so that its boundaries follow the structural domain deformation [30]. These two methods are combined and used to solve the structural problems by Lagrangian formulation. The coupling of the fluid domain and structural domain was attained by using commercial computational software ANSYS. In this research, the fluid and solid are both coupled in a two-way system and solved iteratively within each specified time step of 0.005. The detailed simulation procedure carried out in the current study is represented in figure 8.

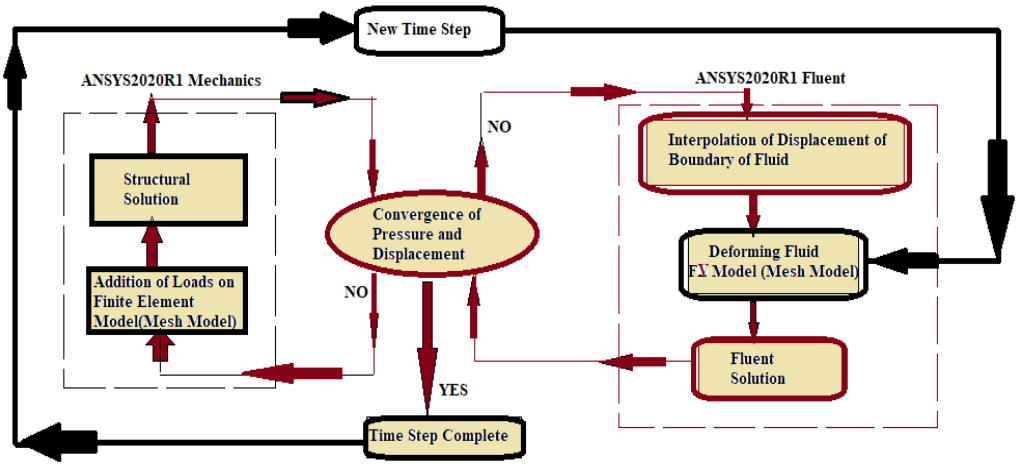

Fig. 8: Flow Chart of Two Way FSI simulation

The FSI problem needs the conservation of mass and momentum along with the interfaces [31]. These values are content by the displacement compatibility and traction equilibrium at $\Gamma_{f,s}$, accordingly to Eq (7) and (8)

$$u_{f,\Gamma} = u_{s,\Gamma} \quad \text{.....7}$$

$$\overrightarrow{t_{f,\Gamma}} = \overrightarrow{t_{s,\Gamma}} \quad \text{.....8}$$

In the above equations, where $u_{f,\Gamma}$ is define the fluid displacement at the interface and $u_{s,\Gamma}$ define the solid displacement at the interface in Eq. (7).

Similarly, the forces of the fluid and solid on the interfaces is defined as $\overrightarrow{t_{f,\Gamma}}$ and $\overrightarrow{t_{s,\Gamma}}$ respectively in Eq. (8) and Eq. (9) is frequently transcribed in stress tensor as,

$$\left(\bar{\bar{\sigma}}_s \cdot \overrightarrow{n_{s,\Gamma}}\right) = \left(p_{f,\Gamma} \cdot \overrightarrow{n_{f,\Gamma}} - \bar{\bar{\tau}}_{f,\Gamma} \cdot \overrightarrow{n_{f,\Gamma}}\right) \text{.....9}$$

Where, $\bar{\bar{\sigma}}_s$ is the stress tensor, $p_{f,\Gamma}$ pressure interface, $\overrightarrow{n_{f,\Gamma}}$ *and* $\overrightarrow{n_{s,\Gamma}}$ are the fluid and solid normal interfaces respectively, $\bar{\bar{\tau}}_{f,\Gamma}$ is the viscous stress tensor.

2.8 Material properties

In the current study, blood was taken as a Non-Newtonian fluid, having density (ρ_f) 1050 kg/m^3 [32,24] . The Carreau model was used for blood viscosity [23]. The viscosity is given as:

$$\mu = \mu_\infty + (\mu_0 - \mu_\infty)[1 + (\lambda\dot{\boldsymbol{\gamma}})^2]^{\frac{(n-1)}{2}} \text{.....10}$$

Where,

λ is the relaxation time, μ_0 is the viscosity at zero shear rate,
μ_∞ is the viscosity for an infinity shear rate
"n" is the power exponent,

In this study, mechanical property of the artery fluid and structural domain was given in table 2. In the current study, the wall of an artery was considered as a linear elastic isotropic material.

Table 2: The detailed properties of the fluid and structural domains

Fluid Properties	**Value**	**Structural Properties**	**Value**
Blood Density(ρ_f)	1050 kg/m^3	Artery Wall Density(ρ_s)	1300 kg/m^3
Viscosity (Shear rate Dependent)	Carreau-model	Linear Elastic Isotropic	
Time Constant lambda (λ) [s],	3.313	Young's Modulus	1.08 (MPa)
Power-Law Index (n)	0.3568	Poisson's ration(υ)	0.49
Zero shear viscosity [Pa s],	0.056(kg/m-s)	Bulk Modulus	1.8E+07 (Pa)
Infinite shear viscosity	0.00345(kg/m-s)	Shear Modulus	3.6242E+05 (Pa)

3. Results

3.1 Effect of stenosis on wall pressure in CFD and FSI models

Figure 9 shows the comparison of wall pressure distribution for CFD and FSI models during the entire cardiac flow. Figure 9 a)b), c)d), e)f), and g)h) represents the early systole, maximum systole, local minimum systole, and beginning of diastole, respectively. It can be seen clearly from figure 9 that the pressure decreases along the direction of flow. The maximum wall pressure of 15180Pa for a rigid model was observed, whereas 14350Pa was noted for the FSI model at the minimum systole. The maximum wall pressure across the LAD and LCX bifurcations for the CFD and FSI model are 14780Pa and 15030Pa during the beginning of the diastole, respectively. The pressure drops for the minimum systolic condition across the stenosis are 14770Pa to 13310Pa and 14350Pa to 13520Pa in CFD and FSI models, respectively. The drop in pressure across the stenosis in CFD and FSI model is 14540Pa to 13320Pa and 14780Pa to 13320Pa during the beginning of the diastole, respectively.

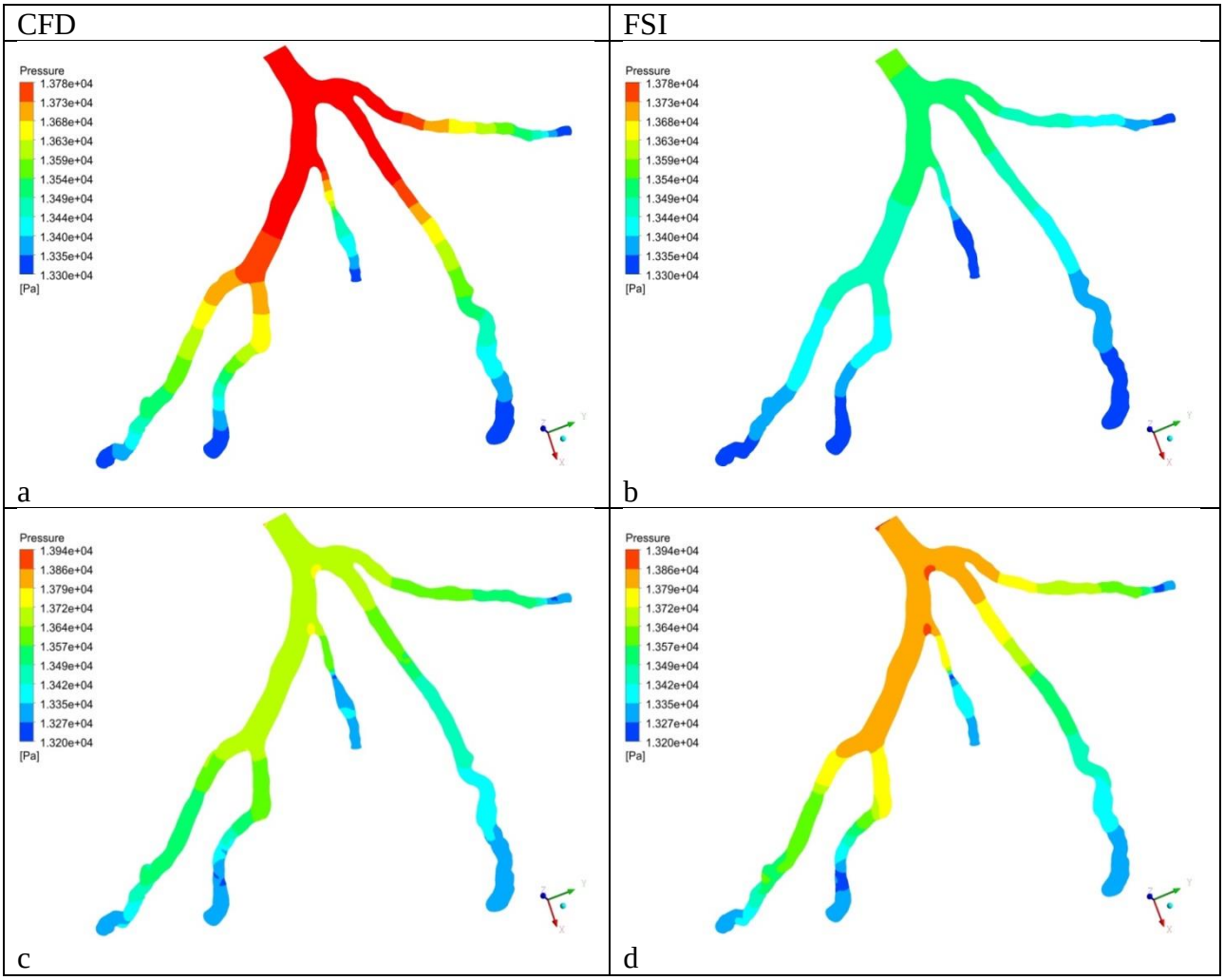

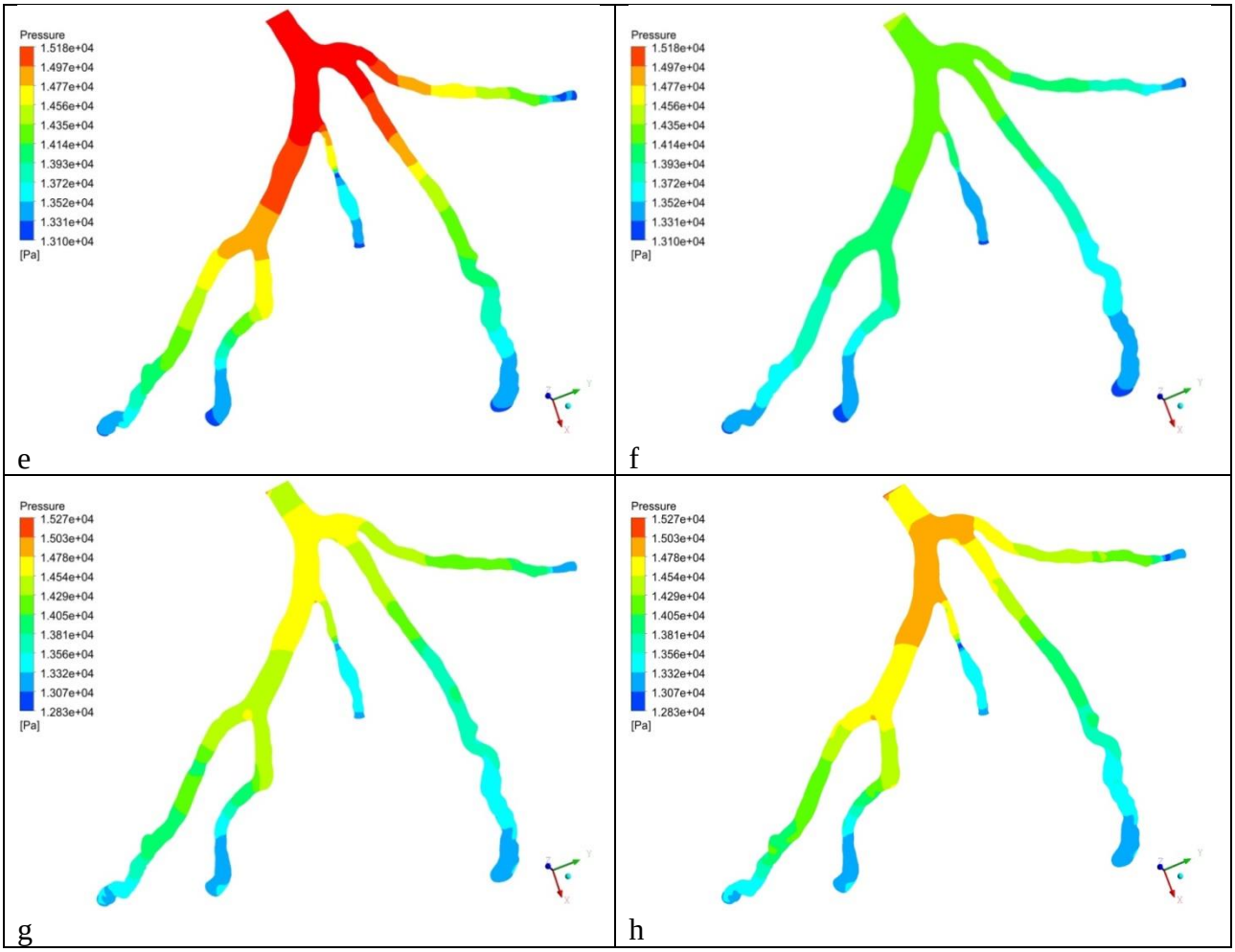

Fig. 9: Comparison between FSI and CFD-computed pressure distribution for coronary artery a)b) early systole (0.3sec) c)d) local maximum systole (0.4sec) e)f) local minimum systole (0.5sec) g)h) beginning of diastole (0.55sec)

3.2 Effect of stenosis on streamline in CFD and FSI models

Figure.10 represents the comparison of velocity streamline distribution for CFD and FSI models during the entire cardiac flow. In figure 10, a)b), c)d), e)f) and g)h) denotes the early systole, maximum systole, local minimum systole, and beginning of diastole, respectively. It can be observed that the velocity is higher at the stenosis. The maximum velocity across the stenosis for maximum peak systole is 0.7751m/s and 0.3972m/s for CFD and FSI, respectively. It is observed that the difference in the velocity magnitude of CFD and FSI studies is mainly found in the region of stenosis. This is justified by the fact that the artery wall is elastic and enlarges with the fluid's pressure, thus increasing the lumen size. For the FSI simulation, as the cross-section increase, velocity decreases.

Similarly, the magnitude of velocity across the stenosis for the maximum diastole is 1.532m/s and 0.443m/s for CFD and FSI, respectively. On comparing the FSI results with the CFD, it is found that the overall magnitude of velocity is higher for the CFD model, which is due to the lesser deformations of the wall brought by the fluid. The obtained results of overall velocity for the model are well within the range of the measurements. A robust secondary flow and recirculation zone at bifurcation regions can be determined during the cardiac cycle for both the CFD and FSI models[34], whereas the recirculation region was found at the post stenosis region, which is consistent with the study published [7].

<table>
<tr><td>CFD</td><td>FSI</td></tr>
<tr><td> 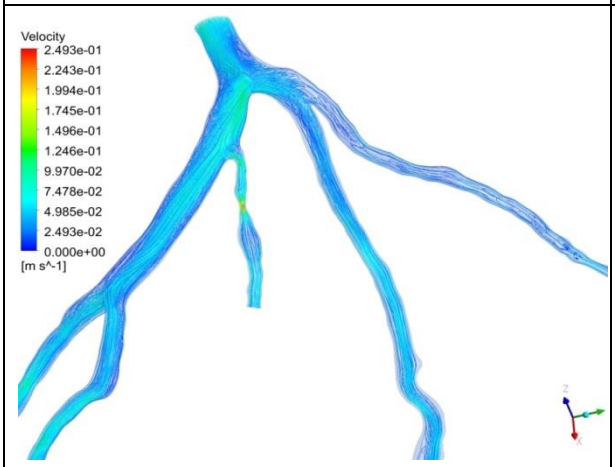

a</td><td> 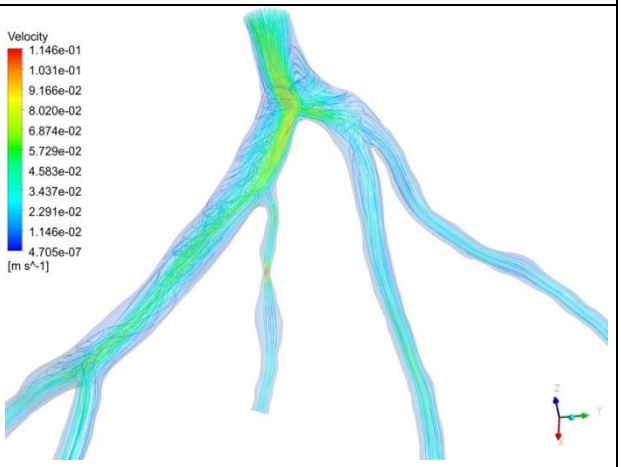

b</td></tr>
<tr><td> 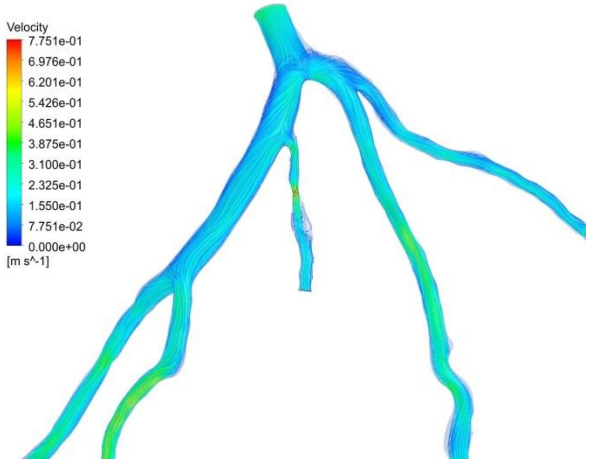

c</td><td> 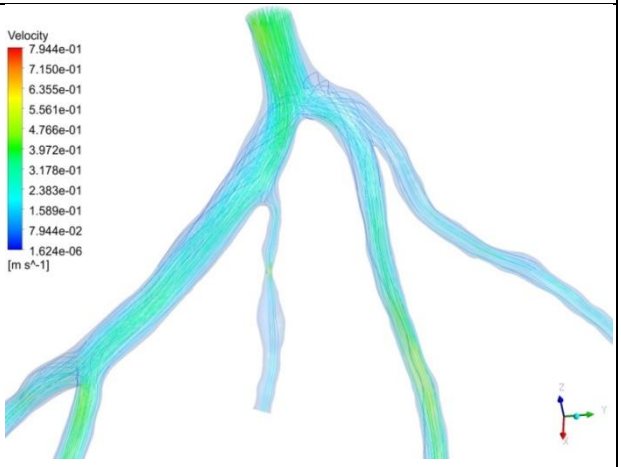

d</td></tr>
</table>

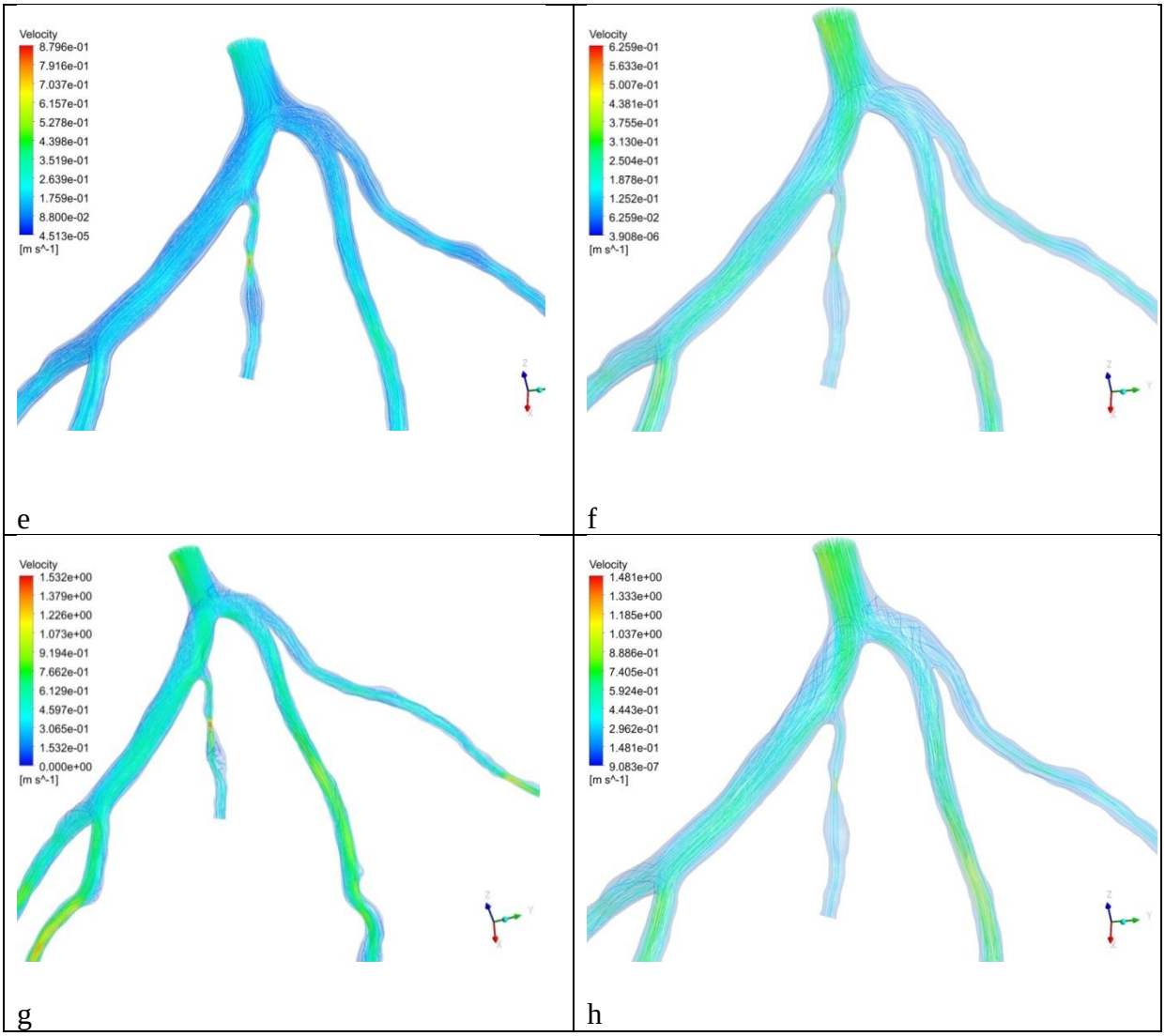

Fig.10: Comparison between FSI and CFD-computed velocity distribution for coronary artery a)b) early systole c)d) maximum systole e)f) local minimum systole g)h) beginning of diastole

3.3 Effect of stenosis on wall shear stress in CFD and FSI models

The wall shear stress (WSS) has great hemodynamics significance, which is very hard to measure directly in vivo. Therefore, computational fluid dynamics provides an alternate way to calculate the WSS in the patient-specific vascular models. It is well known that the low or high area of WSS promotes the progression and development of vascular diseases, including aneurysm, atherosclerosis, and thrombus growth [33]. The endothelial cell layer that presents on the inner surface of the arterial wall is shear-sensitive mechanoreceptors that sense irregular stress and transfer them into biological signals to maintain vascular homeostasis [35]. Figure 11 shows the comparison of wall shear stress distribution for CFD and FSI models at four different time steps of the cardiac cycle. Figure.11 of a)b), c)d), e)f), and g)h)

depicts the early systole, maximum systole, local minimum systole, and beginning of diastole, respectively. It can be seen clearly from figure 11 that the low wall shear found at the period of early systole and higher wall shear stress regions were noted at the beginning of diastole during the cardiac cycle. The results also demonstrated high values of WSS magnitude at the stenosis and the apex of the LAD and LCX bifurcation at the beginning of the diastole. This increased in the magnitude of WSS is due to high-speed flow and velocity gradients across the stenosis. A slight increase in the magnitude of the WSS was observed in CFD models as compared with the FSI model.

CFD	FSI
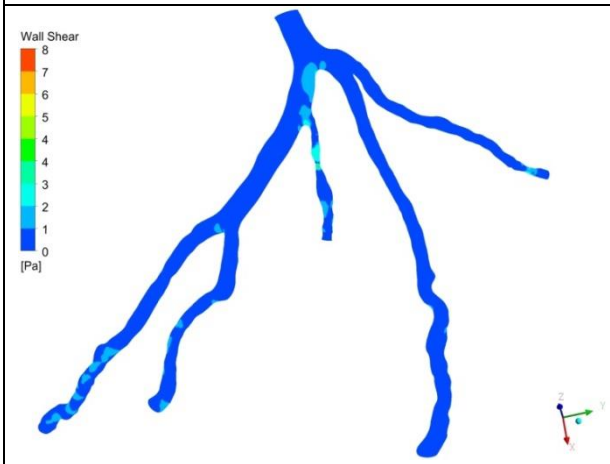 a	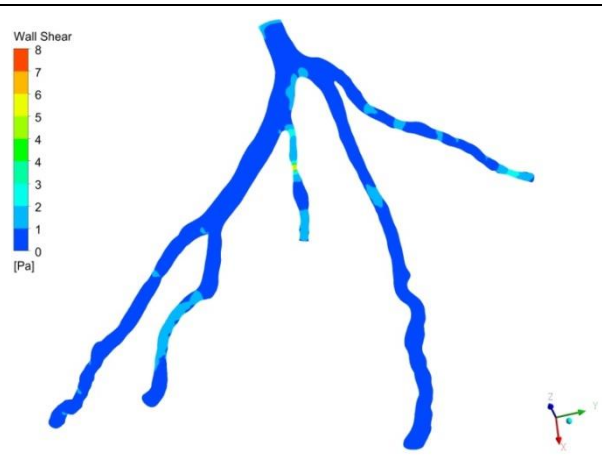 b
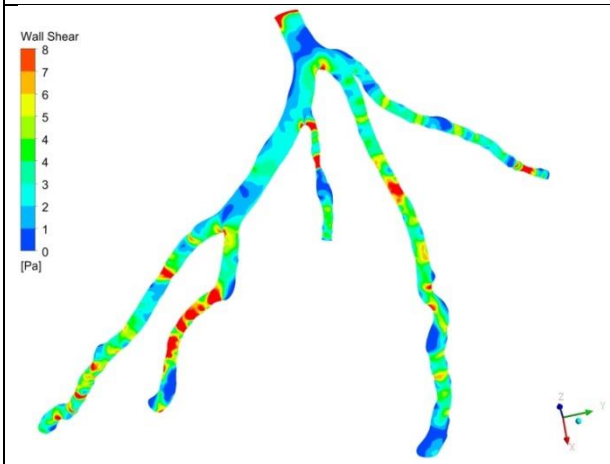 c	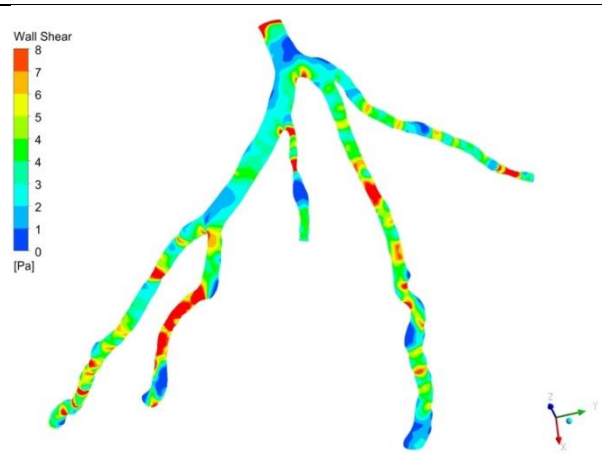 d

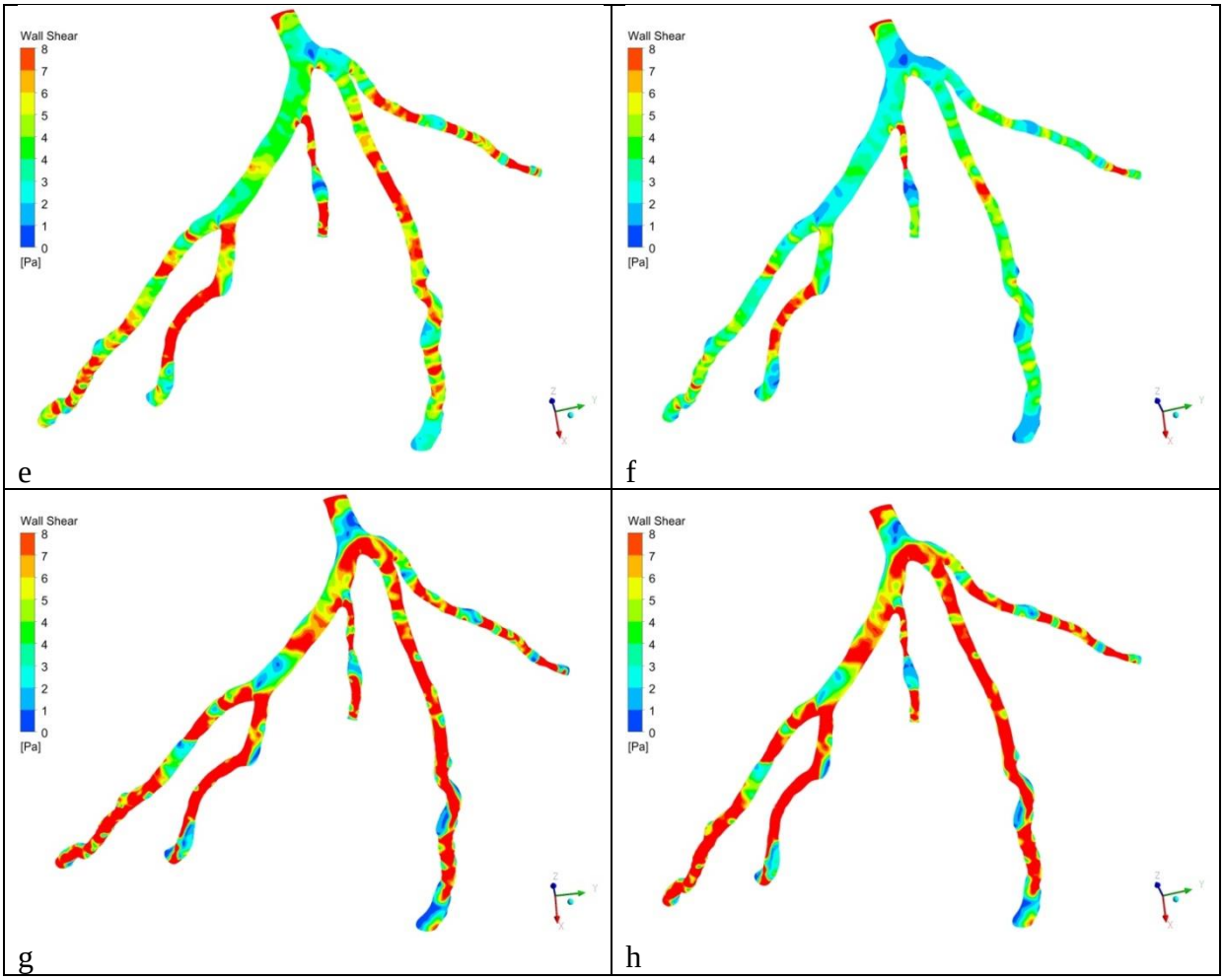

Fig.11: Comparison between CFD and FSI model computed for WSS distribution of left coronary artery a)b) early systole c)d) maximum Systole e)f) local minimum systole g)h) beginning of diastole

3.4 Displacement

Figure 12. shows the front and back face side displacement of the FSI model, computed for the selected time during the cardiac cycle. Figure 12, a), c), e), and g) represents early systole, maximum systole, local minimum systole, and beginning of diastole, respectively. Figure 12 shows the displacement of the arterial wall contours of the FSI studies for the different cardiac cycles. Displacement changes from 0.0015 mm to 0.012 mm in the left coronary artery. The maximum displacement was noted at the branch of the left anterior descending. The minimum displacement was observed across the stenosis, which is due to lower stress imposed by the flow field to the wall.

Front Facing side	Back Facing side
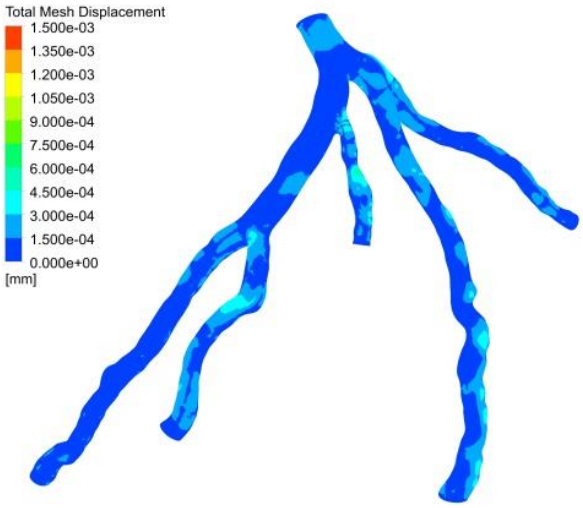 a	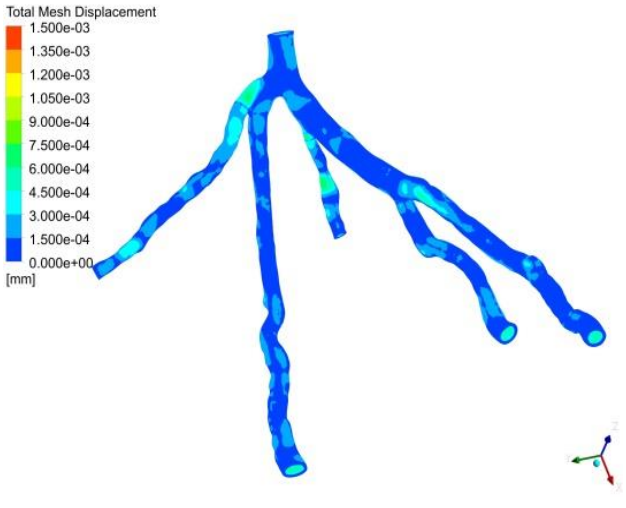 b
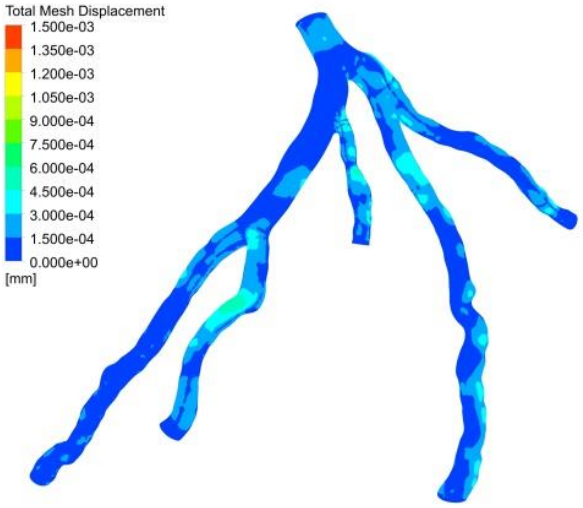 c	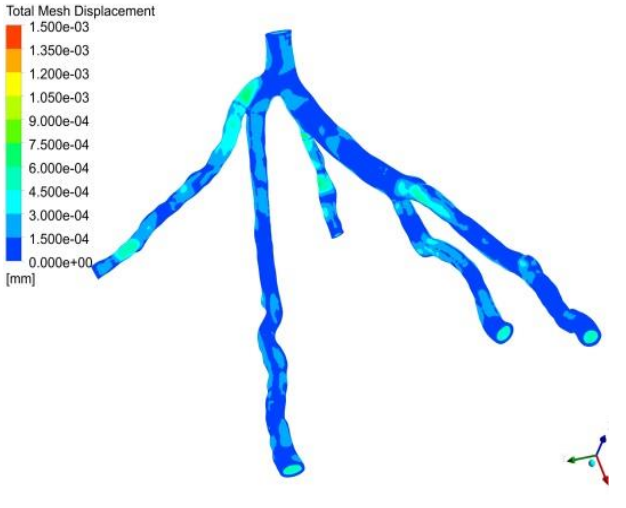 d
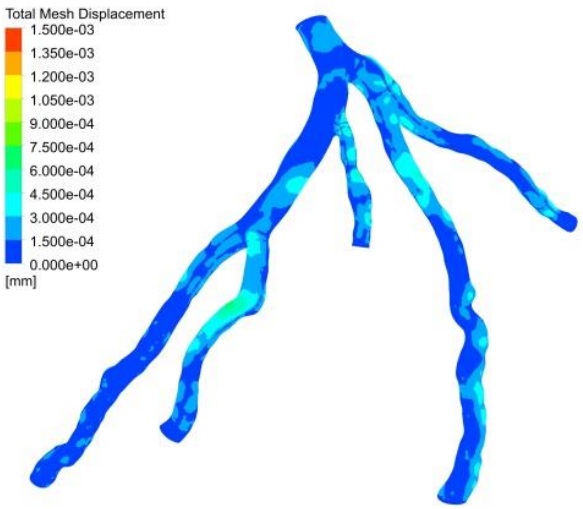 e	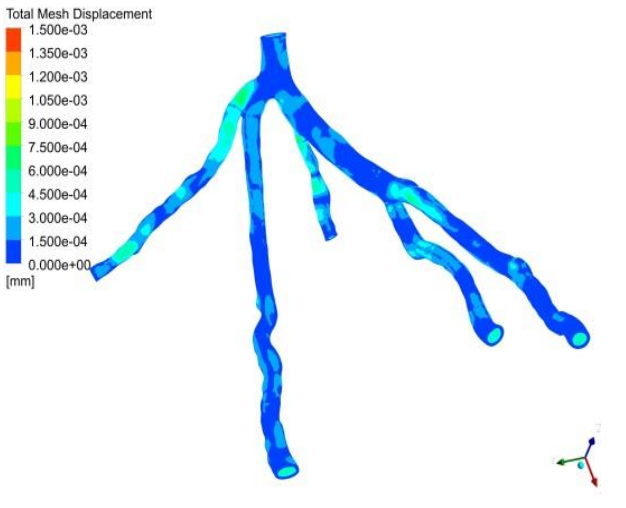 f

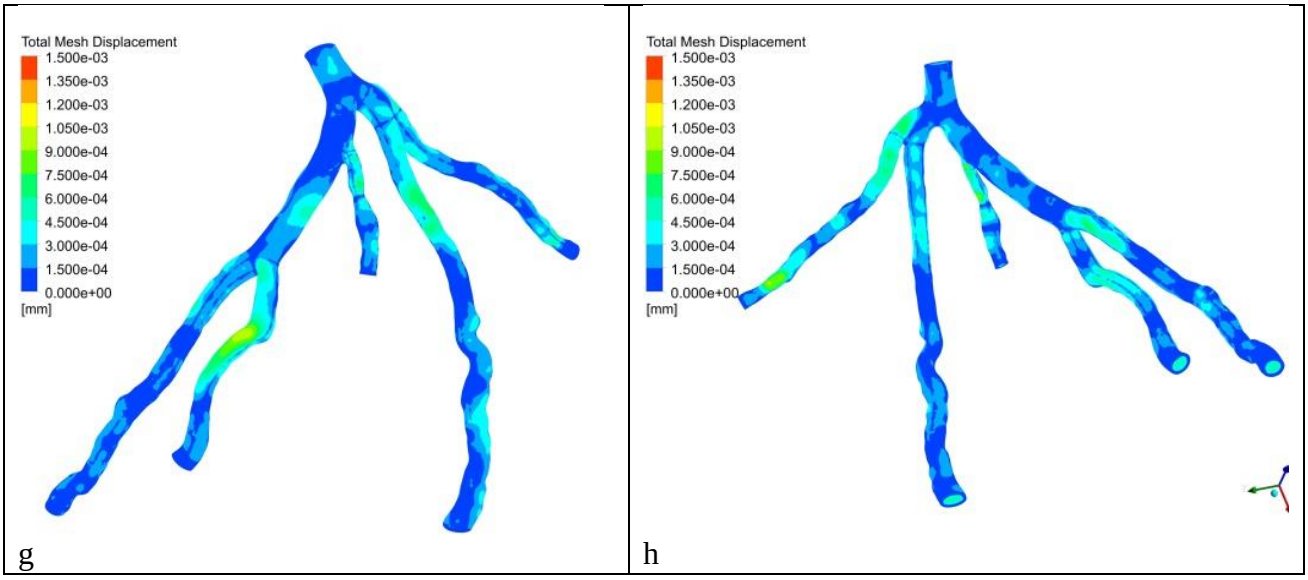

Fig. 12: Displacement counters for the carious cardiac cycle a) early systole, c) maximum systole, e) local minimum systole, and g) beginning of diastole

4. Discussion

In this study, the effect of stenosis on the hemodynamic parameters was investigated with CFD and FSI models for a patient-specific left coronary artery. The pressure drop was observed immediately to the stenosis and found the highest drop for the peak systole. Furthermore, a recirculation zone post stenosis was observed, which could lead to the development of low WSS. The recirculation zone is formed due to low pressure. The absence of adequate blood flow hinders the cleaning of adhesives such as cholesterol, fat, or calcification in that specific region. Thus, it could offer a safe zone for the formation of plaque. The current analysis suggests that the post stenosis could lead to the formation of new stenosis due to the low-velocity region. The wall shear stress had good agreement with the previously published results. The increase in wall shear stress was reported at the stenosis location, and a low WSS was noted immediately after the stenosis[8, 9, 11]. The decrease in WSS augments the creation of reactive oxygen species and increases low-density lipoprotein (LDL) oxidation in the intima layer. The endothelial layer generates the adhesive molecule, such as vascular cell adhesion molecule-1 (VCAM-1) and intracellular adhesion molecule-1 (ICAM-1) by the oxidation process. The platelets were possibly to adhere endothelium layer, where the production of adhesion molecules develops the low WSS region. A slight variation in the instantaneous values of all shear stress was seen in comparing the rigid and FSI models. This can be described by the occurrence of wall deformation, which produces flow and pressure waves which circulate at a finite speed through the arteries, in contrast to the

rigid cases which produce instantaneous wave propagation. For example, it is noted that an increase in WSS area in the CFD model at the local minimum systole when the LCX flow is at its minimum (Figure 11), at which time the CFD wall reacts to the lack of blood supply. In brief, the activation of platelets is related to the increase in the shear stress and harm to endothelial cells; however, the low shear stress is related to the reduction of nitric oxide production and increase endothelin-1 generated by endothelial cells, resulting in the growth of and progression of new stenosis. The results presented in the current study sheds some light on clinical diagnosis of the influence of stenosis upon hemodynamic parameters in patient-specific left coronary artery disease, which could lead to the development of atherosclerosis.

4. Conclusion

The 3D models of the left coronary artery were modeled using CT images, and FSI was performed. The simulation results reveal that the progression and development of atherosclerosis are associated with the harm of the endothelium layer and the hardening of the arteries wall. The velocity and wall shear stress were significantly overestimated in the CFD model as the wall was considered rigid, comparing the CFD and FSI model of the patient-specific left coronary artery with the stenosis. The recirculation region developed immediately after the stenosis creates a low wall shear stress, assisting the stenosis progression. The high wall shear stress developed across the stenosis shoulder leads to the highest risk for stenosis rupture.

Acknowledgment: The authors extend their appréciation to the Deanship of Scientific Research at King Khalid University for funding this work through research groups program under grant number R.G.P 2/105/41.

References

1. Zarins, C.K., Giddens, D.P., Bharadvaj, B., Sottiurai, V.S., Mabon, R.F., Glagov, S.: Carotid bifurcation atherosclerosis. Quantitative correlation of plaque localization with flow velocity profiles and wall shear stress. Circulation research **53**(4), 502-514 (1983).
2. Chatzizisis, Y.S., Coskun, A.U., Jonas, M., Edelman, E.R., Feldman, C.L., Stone, P.H.: Role of endothelial shear stress in the natural history of coronary atherosclerosis and vascular remodeling: molecular, cellular, and vascular behavior. Journal of the American College of Cardiology **49**(25), 2379-2393 (2007).
3. Cecchi, E., Giglioli, C., Valente, S., Lazzeri, C., Gensini, G.F., Abbate, R., Mannini, L.: Role of hemodynamic shear stress in cardiovascular disease. Atherosclerosis **214**(2), 249-256 (2011).

4. Li, Y.-S.J., Haga, J.H., Chien, S.: Molecular basis of the effects of shear stress on vascular endothelial cells. Journal of biomechanics **38**(10), 1949-1971 (2005).
5. Chaichana, T., Sun, Z., Jewkes, J.: Hemodynamic impacts of various types of stenosis in the left coronary artery bifurcation: A patient-specific analysis. Physica Medica **29**(5), 447-452 (2013). doi:http://dx.doi.org/10.1016/j.ejmp.2013.02.001
6. Chaichana, T., Sun, Z., Jewkes, J.: Haemodynamic analysis of the effect of different types of plaques in the left coronary artery. Computerized Medical Imaging and Graphics **37**(3), 197-206 (2013). doi:http://dx.doi.org/10.1016/j.compmedimag.2013.02.001
7. Chaichana, T., Sun, Z., Jewkes, J.: Hemodynamic impacts of left coronary stenosis: A patient-specific analysis. Acta of Bioengineering and Biomechanics **15**(3) (2013).
8. Kamangar, S., Badruddin, I.A., Badarudin, A., Nik-Ghazali, N., Govindaraju, K., Salman Ahmed, N.J., Yunus Khan, T.M.: Influence of stenosis on hemodynamic parameters in the realistic left coronary artery under hyperemic conditions. Computer Methods in Biomechanics and Biomedical Engineering **20**(4), 365-372 (2017). doi:10.1080/10255842.2016.1233402
9. Kamangar, S., Badruddin, I.A., Govindaraju, K., Nik-Ghazali, N., Badarudin, A., Viswanathan, G.N., Ahmed, N.S., Khan, T.Y.: Patient-specific 3D hemodynamics modelling of left coronary artery under hyperemic conditions. Medical & biological engineering & computing **55**(8), 1451-1461 (2017).
10. Steinman, D.A., Thomas, J.B., Ladak, H.M., Milner, J.S., Rutt, B.K., Spence, J.D.: Reconstruction of carotid bifurcation hemodynamics and wall thickness using computational fluid dynamics and MRI. Magnetic Resonance in Medicine: An Official Journal of the International Society for Magnetic Resonance in Medicine **47**(1), 149-159 (2002).
11. Kamangar, S., Badruddin, I.A., Ameer Ahamad, N., Soudagar, M.E.M., Govindaraju, K., Nik-Ghazali, N., Salman Ahmed, N., Khan, Y.: Patient specific 3-d modeling of blood flow in a multi-stenosed left coronary artery. Bio-medical materials and engineering **28**(3), 257-266 (2017).
12. Vallez, L., Sun, B., Plourde, B., Abraham, J., Staniloae, C.: Numerical analysis of arterial plaque thickness and its impact on artery wall compliance. J Cardiovasc Med Cardiol 2 (2): 026-034. DOI: 10.17352/2455 **2976**(026), 55105-51079 (2015).
13. Kleinstreuer, C., Hyun, S., Buchanan, J., Longest, P., Archie Jr, J.P., Truskey, G.A.: Hemodynamic parameters and early intimal thickening in branching blood vessels. Critical Reviews™ in Biomedical Engineering **29**(1) (2001).
14. Zeng, D., Ding, Z., Friedman, M.H., Ethier, C.R.: Effects of cardiac motion on right coronary artery hemodynamics. Annals of biomedical engineering **31**(4), 420-429 (2003).
15. Sousa, L.C., Castro, C.F., António, C.C., Azevedo, E.: Fluid-Structure interaction modelling of blood flow in a non-stenosed common carotid artery bifurcation. In: 7th International Conference on Mechanics and Materials in Design, Albufeira/Portugal 2017
16. Buradi, A., Mahalingam, A.: Numerical Analysis of Wall Shear Stress Parameters of Newtonian Pulsatile Blood Flow Through Coronary Artery and Correlation to Atherosclerosis. In: Advances in Mechanical Engineering. pp. 107-118. Springer, (2020)
17. Buradi, A., Morab, S., Mahalingam, A.: EFFECT OF STENOSIS SEVERITY ON SHEAR-INDUCED DIFFUSION OF RED BLOOD CELLS IN CORONARY ARTERIES. Journal of Mechanics in Medicine and Biology **19**(05), 1950034 (2019).
18. Buradi, A., Mahalingam, A.: Effect of stenosis severity on wall shear stress based hemodynamic descriptors using multiphase mixture theory. J Appl Fluid Mech **11**(6), 1497-1509 (2018).
19. Mahalingam, A., Gawandalkar, U.U., Kini, G., Buradi, A., Araki, T., Ikeda, N., Nicolaides, A., Laird, J.R., Saba, L., Suri, J.S.: Numerical analysis of the effect of turbulence transition on the hemodynamic parameters in human coronary arteries. Cardiovascular diagnosis and therapy **6**(3), 208 (2016).
20. Schwatz, C.R., Fiamoncini, I.A.D., de Sousa, R.N., Bittelbrunn, B.I., da Rosa, L.M., Meier, H.F., Bastos, J.C.S.C.: Evaluation of blood plasma flow around 2D erythrocytes with the use of computational fluid dynamics/Avaliação do escoamento de plasma sanguíneo ao redor de eritrócitos 2D com o uso de fluidodinâmica computacional. Brazilian Journal of Development **5**(8), 11317-11329 (2019).

21. Kamangar, S., Badruddin, I.A., Ahamad, N.A., Govindaraju, K., Nik-Ghazali, N., Ahmed, N., Badarudin, A., Khan, T.: The Influence of Geometrical Shapes of Stenosis on the Blood Flow in Stenosed Artery. Sains Malaysiana **46**(10), 1923-1933 (2017).
22. Kamangar, S., Kalimuthu, G., Anjum Badruddin, I., Badarudin, A., Salman Ahmed, N.J., Khan, T.M.Y.: Numerical Investigation of the Effect of Stenosis Geometry on the Coronary Diagnostic Parameters. The Scientific World Journal **2014**, 7 (2014). doi:10.1155/2014/354946
23. Govindaraju, K., Kamangar, S., Badruddin, I.A., Viswanathan, G.N., Badarudin, A., Salman Ahmed, N.J.: Effect of porous media of the stenosed artery wall to the coronary physiological diagnostic parameter: A computational fluid dynamic analysis. Atherosclerosis **233**(2), 630-635 (2014). doi:http://dx.doi.org/10.1016/j.atherosclerosis.2014.01.043
24. Govindaraju, K., Viswanathan, G.N., Badruddin, I.A., Kamangar, S., Salman Ahmed, N., Al-Rashed, A.A.: The influence of artery wall curvature on the anatomical assessment of stenosis severity derived from fractional flow reserve: a computational fluid dynamics study. Computer methods in biomechanics and biomedical engineering, 1-9 (2016).
25. Secomb, T.W., Ellington, C., Pedley, T.: Mechanics of blood flow in the microcirculation. Biomedical Flows at Low Reynolds Numbers, 9 (1995).
26. Shibeshi, S.S., Collins, W.E.: The rheology of blood flow in a branched arterial system. Applied Rheology **15**(6), 398-405 (2005).
27. Joshi, A.K., Leask, R.L., Myers, J.G., Ojha, M., Butany, J., Ethier, C.R.: Intimal thickness is not associated with wall shear stress patterns in the human right coronary artery. Arteriosclerosis, thrombosis, and vascular biology **24**(12), 2408-2413 (2004).
28. Gijsen, F.J., Wentzel, J.J., Thury, A., Lamers, B., Schuurbiers, J.C., Serruys, P.W., Van der Steen, A.F.: A new imaging technique to study 3-D plaque and shear stress distribution in human coronary artery bifurcations in vivo. Journal of biomechanics **40**(11), 2349-2357 (2007).
29. Donea, J., Giuliani, S., Halleux, J.-P.: An arbitrary Lagrangian-Eulerian finite element method for transient dynamic fluid-structure interactions. Computer methods in applied mechanics and engineering **33**(1-3), 689-723 (1982).
30. Rugonyi, S., Bathe, K.-J.: On finite element analysis of fluid flows fully coupled with structural interactions. CMES- Computer Modeling in Engineering and Sciences **2**(2), 195-212 (2001).
31. Seo, T.: Hemodynamic characteristics in the human carotid artery model induced by blood-arterial wall interactions. International Journal of Biomedical and Biological Engineering **7**(5), 215-220 (2013).
32. Govindaraju, K., Badruddin, I.A., Viswanathan, G.N., Kamangar, S., Ahmed, N.S., Al-Rashed, A.A.: Influence of variable bifurcation angulation and outflow boundary conditions in 3D finite element modelling of left coronary artery on coronary diagnostic parameter. Current Science **111**(2), 368 (2016).
33. Lee, B.-K.: Computational fluid dynamics in cardiovascular disease. Korean circulation journal **41**(8), 423-430 (2011).
34. Chen, X., Zhuang, J., Huang, H. and Wu, Y.: Fluid–structure interactions (FSI) based study of low-density lipoproteins (LDL) uptake in the left coronary artery. Scientific reports 11(1), 1-12. (2021).
35. Jahangiri, M., Saghafian, M., Sadeghi, M.R.: Numerical simulation of hemodynamic parameters of turbulent and pulsatile blood flow in flexible artery with single and double stenoses. Journal of Mechanical Science and Technology **29**(8), 3549-3560 (2015).